

## Vibration damping in sandwich panels

M. R. Maheri · R. D. Adams · J. Hugon

Received: 30 March 2008 / Accepted: 30 April 2008 / Published online: 16 August 2008  
© Springer Science+Business Media, LLC 2008

**Abstract** Currently, there is incomplete knowledge of the damping level and its sources in satellite structures and a suitable method to model it constitutes a necessary step for reliable dynamic predictions. As a first step of a damping characterization, the damping of honeycomb structural panels, which is identified as a main contributor to global damping, has been considered by ALCATEL SPACE. In this work, the inherent vibration damping mechanism in sandwich panels, including those with both aluminium and carbon fibre-reinforced plastic (CFRP) skins, is considered. It is first shown how the theoretical modal properties of the sandwich panel can be predicted from the stiffness and damping properties of its constituent components using the basic laminate theory, a first-order shear deformation theory and a simple discretization method. Next, a finite-element transcription of this approach is presented. It is shown to what extent this method can be implemented using a finite-element software package to predict the overall damping value of a sandwich honeycomb panel for each specific mode. Few of the many theoretical models used to predict natural frequencies of plates are supported by experimental data and even fewer for damping values. Therefore, in a second, experimental part, the Rayleigh–Ritz method and NASTRAN (finite-element

software used by ALCATEL SPACE) predicted modal characteristics (frequency and damping) are compared with the experimentally obtained values for two specimens of typical aluminium core honeycomb panels (aluminium and CFRP skins) used by ALCATEL SPACE as structural panels. It is shown through these results that the method (theoretical and finite element) is satisfactory and promising.

### Introduction

Load-bearing materials are often used in sandwich form in weight-sensitive structures. In this, two skins are attached to a lightweight core such as a “rigid” foam plastic or a honeycomb material. This is primarily to increase the bending stiffness to weight ratio. The tensile modulus of materials is substantially higher than their shear modulus, and this is particularly true with fibre-reinforced plastic (FRP) composites. FRP composites have a high in-plane stiffness to weight ratio. In bending, these composites can be used even more effectively by using sandwich technology.

The disparity between the in-plane and shear elastic moduli of FRP composites also inversely affects their vibration damping capacity: they exhibit substantial damping capacity in shear but are only slightly damped in normal deformation in the fibre direction, although even then they are more damped than metals. It, therefore, follows that the advantage of using FRP composites in a sandwich form for efficient load-bearing does not necessarily carry into utilising their vibration damping capacity. This, however, can sometimes be effectively remedied by employing a damped material for the sandwich core, but there will then usually be stiffness and weight penalties which were not acceptable in the present investigation.

---

M. R. Maheri · R. D. Adams (✉) · J. Hugon  
Mechanical Engineering, University of Bristol, University Walk,  
Bristol BS8 1TR, UK  
e-mail: r.d.adams@bris.ac.uk

J. Hugon  
Alcatel Space, Etablissement de Cannes, 100 Boulevard du Midi,  
BP 99, 06156 Cannes La Bocca Cedex, France

*Present Address:*  
M. R. Maheri  
University of Kerman, Kerman, Iran  
e-mail: MRMaheri@bristolalumni.org.uk

In a previous work [1], it was shown that the basic laminate theory together with a simple numerical procedure, namely the Rayleigh–Ritz method, may be used to predict the modal properties of a thin, laminated FRP panel. The predicted results were shown to correlate favourably with the results obtained experimentally, and were shown to be at least as accurate as the results predicted by the more elaborate finite-element method. The aim in the present work is essentially to build upon that experience, and to investigate the possibility of using an analogous method in trying to predict the modal properties of sandwich panels actually used in aerospace and other transport applications. These are increasingly made from relatively thin and laminated FRP skins and a shear-stiff honeycomb core. Yuan and Dawe [2] and Chen and Chan [3] analysed the vibration of sandwich panels, using numerical solution procedures, while Noor et al. [4] presented a wide-ranging review on computational models for sandwich plates, including vibration and damping. Nayak et al. [5, 6] have used finite-element analysis to predict the vibration modes and damping of simply supported plates, but produced no experimental data to support their findings.

### Theory

#### Preliminary definitions and assumptions

The aim is to determine the modal properties, including frequencies, mode shapes and damping, of a free-free sandwich panel using the numerical method of Rayleigh–Ritz. The measure of damping used here is the specific damping capacity, SDC, defined as the ratio of the energy dissipated in the material to the maximum strain energy reached in one cycle of vibration, thus

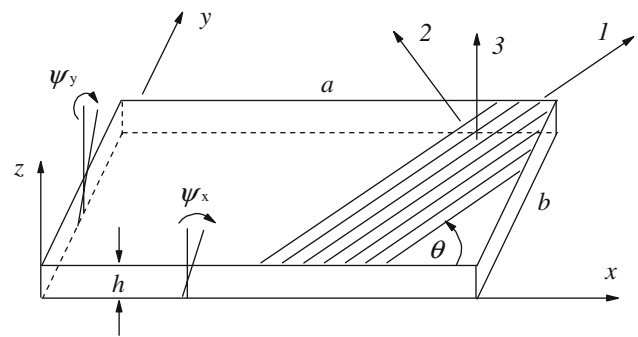
$$\Psi = \frac{\Delta U}{U} \tag{1}$$

$\Psi$  is related to other commonly used damping parameters such that

$$\frac{\Psi}{2\pi} = \eta = \frac{\Delta f}{f_n} = \frac{\delta}{\pi} = \frac{2c}{c_c} = 2\zeta \tag{2}$$

where  $\eta$  is loss factor,  $\delta$  is logarithmic decrement,  $c$  is the viscous damping coefficient,  $\zeta$  is the proportion of critical damping  $c_c$ ,  $f_n$  is the natural frequency and  $\Delta f$  is the bandwidth of the amplitude versus frequency resonance curve at  $1/\sqrt{2}$  of the resonant amplitude.

Chen and Chan [3] used a viscoelastic approach, as did Rikards et al. [7] for predicting the damping of a sandwich plate, but produced no experimental data to validate their results. But it must be pointed out that any frequency [rate] dependence of the damping or moduli of epoxy-based composites and honeycomb cores as used here which are



**Fig. 1** Plate coordinates and lamina orientation: 1, 2 and 3 relate to the fibre direction in a lamina; x, y, and z relate to the major axes of the plate

used at temperatures well below their glass transition temperature is very weak. A strain-rate independent damping mechanism therefore better fits the experimental data for carbon fibre composites and honeycomb [8, 9]. Thus, both of the terms in Eq. 1 can be computed solely from the nature of the modal deformation (mode shape), and the modulus and damping values in the fibre direction and transverse to this direction (axes 1, 2 and 3 in Fig. 1).

It is assumed that there exists mid-plane symmetry through the thickness of the sandwich in terms of material and geometry, and also in terms of the orientation of any orthotropic constituent parts. It is also assumed that the sandwich consists of two uniform skins of high normal stiffness and a uniform core which is of sufficient rigidity to render the sandwich mid-plane as the neutral bending axis of the whole sandwich cross section.

It is further assumed that a Mindlin-type, first-order shear deformation predominates in the sandwich plate, in which case the total rotation of the plate cross sections will consist of not only the rotation due to the bending slope, but also the rotation due to the interlaminar shearing in the plate. In this situation, and for small lateral deformations, a straight line normal to the mid-plane before deformation will remain straight but no longer normal after deformation. We take a simplified approach in estimating the strain energy of a sandwich with thin, layered FRP skins, in that we treat the sandwich as a whole as consisting of ‘layers’ of transversely isotropic materials, albeit of different mechanical properties and geometry. In so doing, however, we apportion the strain energy generated due to the in-plane deformations solely to the skins, and the strain energy generated due to the out-of-plane deformations solely to the core. In effect, the in-plane stresses of the sandwich core, and the transverse shear stresses in the sandwich skin are all assumed to be negligible. The first simplification is only justifiable for a shear-soft sandwich, which is normally the case with practical sandwich materials. The second assumption is only justified when there exists a sufficiently high ratio of the skin/core thickness. It should be emphasised that due to the particularly low interlaminar shear

modulus of the FRP materials, the interlaminar shearing of relatively thick, laminated sandwich skins or, by extension, of thick laminated plates cannot in general be ignored without incurring serious loss of accuracy in the results.

Finally, and in correspondence with an assumed Mindlin-type first-order shear deformation in the two-dimensional plate, we follow the approach taken by Dawe and Roufaeil [10] and by Craig and Dawe [11] in using the equivalent one-dimensional displacement functions, namely the Timoshenko beam equations, in the Rayleigh–Ritz expansions.

On subjecting the plate described above to bending only, one may write

$$u = z\psi_x(x, y) \tag{3a}$$

$$v = z\psi_y(x, y) \tag{3b}$$

$$w = w(x, y) \tag{3c}$$

where  $u$  and  $v$  are displacements at a distance  $z$  through the thickness along the  $x$  and  $y$  directions, respectively,  $w$  is the mid-plane displacement in the  $z$  direction, and  $\psi_x$  and  $\psi_y$  are the total rotations along the  $x$  and  $y$  directions, respectively (Fig. 1).

The in-plane strains are given by

$$\varepsilon_x = \frac{\partial u}{\partial x} \tag{4a}$$

$$\varepsilon_y = \frac{\partial v}{\partial y} \tag{4b}$$

$$\varepsilon_{xy} = \frac{\partial u}{\partial y} + \frac{\partial v}{\partial x} \tag{4c}$$

and the transverse shear strains are given by

$$\varepsilon_{xz} = \frac{\partial u}{\partial z} + \frac{\partial w}{\partial x} = \psi_x + \frac{\partial w}{\partial x} \tag{5a}$$

$$\varepsilon_{yz} = \frac{\partial v}{\partial z} + \frac{\partial w}{\partial y} = \psi_y + \frac{\partial w}{\partial y} \tag{5b}$$

From Eqs. 3–5, it is convenient to write the strains in a compact form as

$$\{\varepsilon_{x,y}\} = \begin{Bmatrix} \varepsilon_x \\ \varepsilon_y \\ \varepsilon_{yz} \\ \varepsilon_{xz} \\ \varepsilon_{xy} \end{Bmatrix} = \begin{Bmatrix} \chi_x z \\ \chi_y z \\ \chi_{yz} \\ \chi_{xz} \\ \chi_{xy} z \end{Bmatrix} \tag{6}$$

where

$$\begin{Bmatrix} \chi_x \\ \chi_y \\ \chi_{yz} \\ \chi_{xz} \\ \chi_{xy} \end{Bmatrix} = \begin{Bmatrix} \frac{\partial \psi_x}{\partial x} \\ \frac{\partial \psi_y}{\partial y} \\ \psi_y + \frac{\partial w}{\partial y} \\ \psi_x + \frac{\partial w}{\partial x} \\ \frac{\partial \psi_x}{\partial y} + \frac{\partial \psi_y}{\partial x} \end{Bmatrix} \tag{7}$$

## Development of the energy expressions

### The strain energy

Denoting the co-ordinate system of any orthotropic material in the sandwich by 1, 2 and 3 (Fig. 1), and assuming that the through-thickness strain is negligible, then the strain energy of the plate is given by

$$U = \frac{1}{2} \int_v \{\sigma_i\}^T \{\varepsilon_i\} dv \quad (i = 1, 2, 4, 5, 6) \tag{8}$$

in which

$$\{\sigma_i\} = [Q_{ij}] \{\varepsilon_j\} \quad (i, j = 1, 2, 4, 5, 6) \tag{9}$$

and

$$\{\varepsilon_i\} = \begin{Bmatrix} \chi_1 z \\ \chi_2 z \\ \chi_4 \\ \chi_5 \\ \chi_6 z \end{Bmatrix} \tag{10}$$

and the matrix  $[Q_{ij}]$  is a symmetric matrix whose components consist of the on-axis, reduced plane stress stiffness matrix ( $i, j = 1, 2, 6$ ), as well as the transverse shear stiffness terms ( $i, j = 4, 5$ ). These are given in terms of the normal and shear moduli,  $E$  and  $G$ , respectively, and of the major Poisson’s ratio  $\nu_{12}$ , as follows

$$\begin{aligned} Q_{11} &= \frac{E_1^2}{E_1 - \nu_{12}^2 E_2}, & Q_{12} &= \frac{\nu_{12} E_1 E_2}{E_1 - \nu_{12}^2 E_2}, \\ Q_{22} &= \frac{E_1 E_2}{E_1 - \nu_{12}^2 E_2}, & Q_{66} &= G_{12}, & Q_{44} & \\ Q_{55} &= G_{13}, & Q_{16} &= Q_{26} = Q_{45} = 0 \end{aligned} \tag{11}$$

It is noted that the suffixes  $i$  and  $j$  correspond to the notations of the fourth-rank stiffness tensor which have been contracted for convenience according to the following scheme

$$11 \rightarrow 1 \quad 22 \rightarrow 2 \quad 33 \rightarrow 3 \quad 23 \rightarrow 4 \quad 13 \rightarrow 5 \quad 12 \rightarrow 6.$$

Substituting for  $\{\sigma_i\}$  from Eq. 9 and for  $\{\varepsilon_i\}$  from Eq. 10 in Eq. 8 gives

$$U = \frac{1}{2} \int_v \begin{Bmatrix} \chi_1 z \\ \chi_2 z \\ \chi_4 \\ \chi_5 \\ \chi_6 z \end{Bmatrix}^T \{Q_{ij}\} \begin{Bmatrix} \chi_1 z \\ \chi_2 z \\ \chi_4 \\ \chi_5 \\ \chi_6 z \end{Bmatrix} dv \tag{12}$$

Using the strain transformation relationship

$$\{\varepsilon_i\} = [T] \{\varepsilon_{x,y}\}, \tag{13}$$

in which  $[T]$  is given in terms of directional cosine terms  $m = \cos \theta$ ,  $n = \sin \theta$  as

$$[T] = \begin{bmatrix} m^2 & n^2 & 0 & 0 & mn \\ n^2 & m^2 & 0 & 0 & -mn \\ 0 & 0 & m & -n & 0 \\ 0 & 0 & n & m & 0 \\ -2mn & 2mn & 0 & 0 & m^2 - n^2 \end{bmatrix}, \tag{14}$$

then the strain energy in the plate co-ordinate system is given by

$$U = \frac{1}{2} \int_v \left\{ [T] \begin{Bmatrix} \chi_{xz} \\ \chi_{yz} \\ \chi_{xz} \\ \chi_{xy} \end{Bmatrix} \right\}^T \{ [Q_{ij}] [T] \begin{Bmatrix} \chi_{xz} \\ \chi_{yz} \\ \chi_{xz} \\ \chi_{xy} \end{Bmatrix} \} dv$$

$$= \frac{1}{2} \int_v \left\{ \begin{Bmatrix} \chi_{xz} \\ \chi_{yz} \\ \chi_{xz} \\ \chi_{xy} \end{Bmatrix} \right\}^T \{ \bar{[Q]}_{ij} \begin{Bmatrix} \chi_{xz} \\ \chi_{yz} \\ \chi_{xz} \\ \chi_{xy} \end{Bmatrix} \} dv \tag{15}$$

where

$$\bar{[Q]}_{ij} = [T]^T [Q_{ij}] [T] \tag{16}$$

Noting that slopes and deflections are invariant of  $z$ , then Eq. 15 can be simplified to

$$U = \frac{1}{2} \int_{\Omega} \left( \begin{bmatrix} \chi_x \\ \chi_y \\ \chi_{xy} \end{bmatrix}^T (D_{ij}) \begin{bmatrix} \chi_x \\ \chi_y \\ \chi_{xy} \end{bmatrix} \right) (i, j = 1, 2, 6)$$

$$+ \left\{ \begin{bmatrix} \chi_{yz} \\ \chi_{xz} \end{bmatrix}^T (A_{ij}) \begin{bmatrix} \chi_{yz} \\ \chi_{xz} \end{bmatrix} \right\} (i, j = 4, 5) \tag{17}$$

in which  $\Omega$  is the plate surface area and,

$$[D_{ij}] = \int_{-h/2}^{h/2} \bar{[Q]}_{ij} z^2 dz \quad (i, j = 1, 2, 6) \tag{18}$$

Since  $\bar{Q}_{ij}$  is independent of  $z$  within each layer  $k$ , this equation may be written as

$$[D_{ij}] = \sum_{k=1}^L \bar{[Q]}_{ij}^k \int_{h_{(k-1)}}^{h_k} z^2 dz = \frac{1}{3} \sum_{k=1}^L \bar{[Q]}_{ij}^k (h_k^3 - h_{(k-1)}^3)$$

$$(i, j = 1, 2, 6) \tag{19}$$

in which  $\bar{Q}_{ij}^{(k)}$  is the off-axis reduced plane stress stiffness matrix of the  $k$ th layer,  $h_k$  and  $h_{(k-1)}$  are the upper and lower  $z$ -coordinates of the  $k$ th layer, respectively, and  $L$  is the total number of layers. For the mid-plane symmetric plate the following hold

$$\theta(Z) = \theta(-Z) \quad \text{and} \quad \bar{Q}_{ij}^k(Z) = \bar{Q}_{ij}^k(-Z) \tag{20}$$

Then, Eq. 19 may be simplified to

$$[D_{ij}] = \frac{2}{3} \sum_{k=1}^{L/2} \bar{[Q]}_{ij}^k (h_k^3 - h_{(k-1)}^3) \quad (i, j = 1, 2, 6) \tag{21}$$

Ignoring the transverse shear in the skins, and letting  $h_c$  be the total thickness of the core, then

$$[A_{ij}] = \int_{-h_c/2}^{h_c/2} \bar{[Q]}_{ij} dz = h_c \bar{[Q]}_{ij}^c \quad (i, j = 4, 5) \tag{22}$$

in which  $\bar{[Q]}_{ij}^c$  corresponds to the core.

Using Eq. 7 in Eq. 17, expanding and simplifying the resulting expressions gives

$$U = \frac{1}{2} \int_{\Omega} \left( D_{11} \left( \frac{\partial \psi_x}{\partial x} \right)^2 + 2D_{12} \frac{\partial \psi_x}{\partial x} \frac{\partial \psi_y}{\partial y} \right.$$

$$+ 2D_{16} \frac{\partial \psi_x}{\partial x} \left( \frac{\partial \psi_x}{\partial y} + \frac{\partial \psi_y}{\partial x} \right) + D_{22} \left( \frac{\partial \psi_y}{\partial y} \right)^2$$

$$+ 2D_{26} \frac{\partial \psi_y}{\partial y} \left( \frac{\partial \psi_x}{\partial y} + \frac{\partial \psi_y}{\partial x} \right) + D_{66} \left( \frac{\partial \psi_x}{\partial y} + \frac{\partial \psi_y}{\partial x} \right)^2$$

$$+ A_{44} \left( \psi_y + \frac{\partial w}{\partial y} \right)^2 + A_{55} \left( \psi_x + \frac{\partial w}{\partial x} \right)^2$$

$$\left. + 2A_{45} \left( \psi_x \psi_y + \psi_x \frac{\partial w}{\partial y} + \psi_y \frac{\partial w}{\partial x} + \frac{\partial w}{\partial x} \frac{\partial w}{\partial y} \right) \right) d\Omega \tag{23}$$

*The damping energy*

Assuming that the damping energy is the sum of separable energy dissipations due to the individual stress components [12], then the total dissipated energy for the five stress components considered in the present analysis is given by

$$\Delta U = \frac{1}{2} \int_v \{ \sigma_i \}^T [\psi] \{ \varepsilon_i \} dv \quad (i = 1, 2, 4, 5, 6) \tag{24}$$

where the damping matrix  $[\psi]$  is the diagonal matrix

$$[\psi] = \begin{bmatrix} \psi_1 & & & & & \\ & \psi_2 & & & & \\ & & \psi_4 & & & \\ & & & \psi_5 & & \\ & & & & \psi_6 & \end{bmatrix}, \tag{25}$$

whose components quantify the proportion of the energy loss in each cycle of vibration due to each stress component.

The development of the expression for damping energy in Eq. 24 is similar to that for the strain energy, and it will not be reproduced here for brevity reasons. On developing the expression (24), and in analogy with

the expression obtained for the strain energy in Eq. 23, the following expression is obtained for the damping energy

$$\begin{aligned} \Delta U = & \frac{1}{2} \int_{\Omega} \left( d_{11} \left( \frac{\partial \psi_x}{\partial x} \right)^2 + (d_{12} + d_{21}) \frac{\partial \psi_x}{\partial x} \frac{\partial \psi_y}{\partial y} \right. \\ & + (d_{16} + d_{61}) \frac{\partial \psi_x}{\partial x} \left( \frac{\partial \psi_x}{\partial y} + \frac{\partial \psi_y}{\partial x} \right) + d_{22} \left( \frac{\partial \psi_y}{\partial y} \right)^2 \\ & + (d_{26} + d_{62}) \frac{\partial \psi_y}{\partial y} \left( \frac{\partial \psi_x}{\partial y} + \frac{\partial \psi_y}{\partial x} \right) + d_{66} \left( \frac{\partial \psi_x}{\partial y} + \frac{\partial \psi_y}{\partial x} \right)^2 \\ & + d_{44} \left( \psi_y + \frac{\partial w}{\partial y} \right)^2 + d_{55} \left( \psi_x + \frac{\partial w}{\partial x} \right)^2 \\ & \left. + (d_{45} + d_{54}) \left( \psi_x \psi_y + \psi_x \frac{\partial w}{\partial y} + \psi_y \frac{\partial w}{\partial x} + \frac{\partial w}{\partial x} \frac{\partial w}{\partial y} \right) \right) d\Omega \end{aligned} \tag{26}$$

where

$$[d_{ij}] = \frac{2}{3} \sum_{k=1}^{L/2} [\bar{R}_{ij}^k] (h_k^3 - h_{(k-1)}^3) \quad (i, j = 1, 2, 6) \tag{27}$$

and

$$[d_{ij}] = h_c [\bar{R}_{ij}^c] \quad (i, j = 4, 5) \tag{28}$$

in which  $[\bar{R}_{ij}^c]$  corresponds to the core. The damped stiffness matrix  $[\bar{R}_{ij}]$  is a generally non-symmetric matrix whose components are given as

$$[\bar{R}_{ij}] = [T]^T [\psi][Q_{ij}][T] \quad (i, j = 1, 2, 4, 5, 6) \tag{29}$$

The Rayleigh–Ritz energy minimization method

The Rayleigh–Ritz method is covered extensively in the literature. A detailed account for isotropic plates has been given by Young [13] and for anisotropic plates by Ashton and Waddoups [14] and by Ashton and Whitney [15]. The method involves expressing the lateral deflection of a rectangular plate in terms of suitable beam functions in the  $x$  and  $y$  directions. On subsequent minimisation of the total energy of the plate, the plate modal properties including modal frequency and deformations (mode shapes) are obtained.

The Rayleigh–Ritz trial functions in the present case are given by Craig and Dawe [11] as

$$w(x, y) = \sum_{m=1}^M \sum_{n=1}^N a_{mn} w_m(x) w_n(y) \tag{30a}$$

$$\psi_x(x, y) = \sum_{m=1}^M \sum_{n=1}^N b_{mn} \psi_m(x) w_n(y) \tag{30b}$$

$$\psi_y(x, y) = \sum_{m=1}^M \sum_{n=1}^N c_{mn} w_m(x) \psi_n(y) \tag{30c}$$

in which  $a_{mn}$ ,  $b_{mn}$  and  $c_{mn}$  are unknown coefficients to be determined through the minimisation of energy, and  $w$  and  $\psi$  are the Timoshenko beam functions satisfying the free-free boundary conditions (these are the boundary conditions applicable to the present work)

$$w = (\cosh(b\alpha\xi) + \delta \sinh(b\alpha\xi) + \theta \cos(b\beta\xi) + (-\lambda\delta) \sin(b\beta\xi)) \quad (x/y) \tag{31a}$$

$$\psi = (\delta k_2 \cosh(b\alpha\xi) + k_2 \sinh(b\alpha\xi) + (-\lambda\delta k_1) \cos(b\beta\xi) + (-\theta k_1) \sin(b\beta\xi)) \quad (x/y) \tag{31b}$$

where the  $(x/y)$  notation is meant to indicate that the functions are applied in both  $x$  and  $y$  directions, and

$$\xi = \frac{x, y}{L_{x/y}},$$

$$\alpha, \beta = (1/\sqrt{2}) \left\{ -, +(r^2 + s^2) + \left[ (r^2 - s^2) + \frac{4}{b^2} \right]^{\frac{1}{2}} \right\}^{\frac{1}{2}},$$

$$k_1 = b(\beta^2 - s^2)/\beta L, \quad k_2 = b(\alpha^2 + s^2)/\alpha L, \quad \theta = \frac{k_2 \alpha}{k_1 \beta},$$

$$\lambda = \frac{b\alpha - k_2}{b\beta - k_1}$$

$$r^2 = \frac{I}{AL^2}, \quad s^2 = \frac{EI}{kAGL^2}, \quad \delta = \frac{\cos(b\beta) - \cosh(b\alpha)}{(\lambda/\theta) \sin(b\beta) - \sinh(b\alpha)} \tag{32}$$

in which  $b$  (not to be confused with  $b$  representing the plate width) is the roots of the frequency equation of the free-free Timoshenko beam, which is given as

$$2 - 2\cosh(b\alpha) \cos(b\beta) + b \frac{[b^2 r^2 (r^2 - s^2)^2 + 3r^2 - s^2]}{\sqrt{(1 - b^2 r^2 s^2)}} \sinh(b\alpha) \sin(b\beta) = 0 \quad (x/y) \tag{33}$$

It is noted that the first two rigid body modes of the free-free beam are given by

$$(1) \left\{ \begin{matrix} w_1 = 1 \\ w_2 = 1 - 2\xi \end{matrix} \right\}, \quad \text{and} \quad (2) \left\{ \begin{matrix} \psi_1 = 0 \\ \psi_2 = 1 \end{matrix} \right\} \tag{34}$$

Following the substitution of the trial functions (30) in Eq. 23, and rearranging the resulting expression so that the

functions of  $x$  and  $y$  are separated into their respective integration domains, one can obtain the strain energy

By comparing Eq. 26 with Eq. 23, it is easily verified that the expression for the damping energy following the

$$\begin{aligned}
 U = & \frac{1}{2} \sum_{i=1}^M \sum_{j=1}^N \left\{ D_{11} \left[ b_{ij} \int_a \psi'_i \psi'_m dx \int_b w_j w_n dy \right] b_{mn} + 2D_{12} \left[ b_{ij} \int_a \psi'_i w_m dx \int_b w_j \psi'_n dy \right] c_{mn} \right. \\
 & + 2D_{16} \left\{ \left[ b_{ij} \int_a \psi'_i \psi'_m dx \int_b w_j w'_n dy \right] b_{mn} + \left[ b_{ij} \int_a \psi'_i w'_m dx \int_b w_j \psi_n dy \right] c_{mn} \right\} \\
 & + D_{22} \left[ c_{ij} \int_a w_i w_m dx \int_b \psi'_j \psi'_n dy \right] c_{mn} + 2D_{26} \left\{ \left[ c_{ij} \int_a w_i \psi_m dx \int_b \psi'_j w'_n dy \right] b_{mn} \right. \\
 & + \left. \left[ c_{ij} \int_a w_i w'_m dx \int_b \psi'_j \psi_n dy \right] c_{mn} \right\} + D_{66} \left\{ \left[ b_{ij} \int_a \psi_i \psi_m dx \int_b w'_j w'_n dy \right] b_{mn} \right. \\
 & + \left. \left[ c_{ij} \int_a w'_i w'_m dx \int_b \psi_j \psi_n dy \right] c_{mn} + 2 \left[ b_{ij} \int_a \psi_i w'_m dx \int_b w'_j \psi_n dy \right] c_{mn} \right\} \\
 & + A_{44} \left\{ \left[ c_{ij} \int_a w_i w_m dx \int_b \psi_j \psi_n dy \right] c_{mn} + \left[ a_{ij} \int_a w_i w_m dx \int_b w'_j w'_n dy \right] a_{mn} \right. \\
 & + 2 \left. \left[ c_{ij} \int_a w_i w_m dx \int_b \psi_j w'_n dy \right] a_{mn} \right\} + A_{55} \left\{ \left[ b_{ij} \int_a \psi_i \psi_m dx \int_b w_j w_n dy \right] b_{mn} \right. \\
 & + \left. \left[ a_{ij} \int_a w'_i w'_m dx \int_b w_j w_n dy \right] a_{mn} + 2 \left[ b_{ij} \int_a \psi_i w'_m dx \int_b w_j w_n dy \right] a_{mn} \right\} \\
 & + 2A_{45} \left\{ \left[ b_{ij} \int_a \psi_i w_m dx \int_b w_j \psi_n dy \right] c_{mn} + \left[ b_{ij} \int_a \psi_i w_m dx \int_b w_j w'_n dy \right] a_{mn} \right. \\
 & + \left. \left[ c_{ij} \int_a w_i w'_m dx \int_b \psi_j w_n dy \right] a_{mn} + \left[ a_{ij} \int_a w'_i w_m dx \int_b w_j w'_n dy \right] a_{mn} \right\} \\
 & \left. \right\} \\
 & (m = 1, 2, \dots, M; \quad n = 1, 2, \dots, N)
 \end{aligned}
 \tag{35}$$

Rayleigh–Ritz expansion procedure becomes essentially the same as the expression for the strain energy once appropriate substitutions of the factors  $d$  for the factors  $D$  and  $A$  in this latter equation are made

Finally, the kinetic energy is given by

$$T = \frac{1}{2} \int_{\Omega} \left( \rho h w^2 + \rho \frac{h^3}{12} (\psi_x^2 + \psi_y^2) \right) d\Omega \cdot \omega^2 \quad (37)$$

$$\begin{aligned} \Delta U = & \frac{1}{2} \sum_{i=1}^M \sum_{j=1}^N \left\{ d_{11} \left[ b_{ij} \int_a \psi'_i \psi'_m dx \int_b w_j w_n dy \right] b_{mn} + (d_{12} + d_{21}) \left[ b_{ij} \int_a \psi'_i w_m dx \int_b w_j \psi'_n dy \right] c_{mn} \right. \\ & + (d_{16} + d_{61}) \left\{ \left[ b_{ij} \int_a \psi'_i \psi_m dx \int_b w_j w'_n dy \right] b_{mn} + \left[ b_{ij} \int_a \psi'_i w'_m dx \int_b w_j \psi_n dy \right] c_{mn} \right\} \\ & + d_{22} \left[ c_{ij} \int_a w_i w_m dx \int_b \psi'_j \psi'_n dy \right] c_{mn} + (d_{26} + d_{62}) \left\{ \left[ c_{ij} \int_a w_i \psi_m dx \int_b \psi'_j w'_n dy \right] b_{mn} \right. \\ & + \left. \left[ c_{ij} \int_a w_i w'_m dx \int_b \psi'_j \psi_n dy \right] c_{mn} \right\} + d_{66} \left\{ \left[ b_{ij} \int_a \psi_i \psi_m dx \int_b w'_j w'_n dy \right] b_{mn} \right. \\ & + \left. \left[ c_{ij} \int_a w'_i w'_m dx \int_b \psi_j \psi_n dy \right] c_{mn} + 2 \left[ b_{ij} \int_a \psi_i w'_m dx \int_b w'_j \psi_n dy \right] c_{mn} \right\} \\ & + d_{44} \left\{ \left[ c_{ij} \int_a w_i w_m dx \int_b \psi_j \psi_n dy \right] c_{mn} + \left[ a_{ij} \int_a w_i w_m dx \int_b w'_j w'_n dy \right] a_{mn} \right. \\ & + 2 \left. \left[ c_{ij} \int_a w_i w_m dx \int_b \psi_j w'_n dy \right] a_{mn} \right\} + d_{55} \left\{ \left[ b_{ij} \int_a \psi_i \psi_m dx \int_b w_j w_n dy \right] b_{mn} \right. \\ & + \left. \left[ a_{ij} \int_a w'_i w'_m dx \int_b w_j w_n dy \right] a_{mn} + 2 \left[ b_{ij} \int_a \psi_i w'_m dx \int_b w_j w_n dy \right] a_{mn} \right\} \\ & + (d_{45} + d_{54}) \left\{ \left[ b_{ij} \int_a \psi_i w_m dx \int_b w_j \psi_n dy \right] c_{mn} + \left[ b_{ij} \int_a \psi_i w_m dx \int_b w_j w'_n dy \right] a_{mn} \right. \\ & + \left. \left[ c_{ij} \int_a w_i w'_m dx \int_b \psi_j w_n dy \right] a_{mn} + \left[ a_{ij} \int_a w'_i w_m dx \int_b w_j w'_n dy \right] a_{mn} \right\} \left. \right\} \\ & (m = 1, 2, \dots, M; \quad n = 1, 2, \dots, N) \end{aligned} \quad (36)$$



In a similar manner, following the substitution of the trial functions (30) in Eq. 37 and rearranging so that the functions of  $x$  and  $y$  are separated into their respective integration domains, the following expression can be obtained for the kinetic energy

$$T = \frac{1}{2} \sum_{i=1}^M \sum_{j=1}^N \left\{ \rho h \left[ a_{ij} \int_a w_i w_m dx \int_b w_j w_n dy \right] a_{mn} + \rho \frac{h^3}{12} \left\{ \left[ b_{ij} \int_a \psi_i \psi_m dx \int_b w_j w_n dy \right] b_{mn} + \left[ c_{ij} \int_a w_i w_m dx \int_b \psi_j \psi_n dy \right] c_{mn} \right\} \right\} \cdot \omega^2$$

Since the total energy of the system is constant at any given time, i.e.,

$$U - T = \text{constant}, \tag{38}$$

then it follows that

$$\begin{bmatrix} \frac{\partial(U-T)}{\partial a_{ij}} \\ \frac{\partial(U-T)}{\partial b_{ij}} \\ \frac{\partial(U-T)}{\partial c_{ij}} \end{bmatrix} = 0 \tag{39}$$

Writing

$$\begin{bmatrix} \frac{\partial U}{\partial a_{ij}} \\ \frac{\partial U}{\partial b_{ij}} \\ \frac{\partial U}{\partial c_{ij}} \end{bmatrix} = \begin{bmatrix} C_{11} & C_{12} & C_{13} \\ C_{21} & C_{22} & C_{23} \\ C_{31} & C_{32} & C_{33} \end{bmatrix} \begin{bmatrix} a_{mn} \\ b_{mn} \\ c_{mn} \end{bmatrix} \tag{40}$$

and

$$\begin{bmatrix} \frac{\partial T}{\partial a_{ij}} \\ \frac{\partial T}{\partial b_{ij}} \\ \frac{\partial T}{\partial c_{ij}} \end{bmatrix} = \omega^2 \begin{bmatrix} m_{11} & & 0 \\ & m_{22} & \\ 0 & & m_{33} \end{bmatrix} \begin{bmatrix} a_{mn} \\ b_{mn} \\ c_{mn} \end{bmatrix}, \tag{41}$$

then Eq. 39 can be written as

$$\begin{bmatrix} \frac{\partial(U-T)}{\partial a_{ij}} \\ \frac{\partial(U-T)}{\partial b_{ij}} \\ \frac{\partial(U-T)}{\partial c_{ij}} \end{bmatrix} = \begin{bmatrix} (C_{11} - \omega^2 m_{11}) & C_{12} & C_{13} \\ C_{21} & (C_{22} - \omega^2 m_{22}) & C_{23} \\ C_{31} & C_{32} & (C_{33} - \omega^2 m_{33}) \end{bmatrix} \times \begin{bmatrix} a_{mn} \\ b_{mn} \\ c_{mn} \end{bmatrix} = 0 \tag{42}$$

The terms for  $C_{ij}$  and  $m_{ii}$  will be found in the Appendix.

Equation (42) can be written in the generalised eigenvalue problem form in terms of stiffness and mass

matrices  $\mathbf{K}$  and  $\mathbf{M}$ , respectively, and of displacements  $\mathbf{A}$  as

$$(\mathbf{K} - \omega^2 \mathbf{M})\mathbf{A} = 0 \tag{43}$$

On pre-multiplying this equation by  $\mathbf{K}^{-1}$ , and rearranging to give

$$\mathbf{K}^{-1} \mathbf{M} \mathbf{A} = \Lambda \mathbf{A} \tag{44}$$

in which  $\Lambda = 1/\omega^2$ , then the solution of Eq. 44 by an iterative method will yield the modal characteristics, including angular frequencies  $\omega$  and generalised displacements  $\mathbf{A}$ , starting with the more prominent, lower modes.

For any generalised modal displacements  $\mathbf{A}$  so obtained, the modal specific damping capacity can be computed from either Eqs. 1, 35 and 36 or, alternatively, from Eqs. 1, 36 and 37 since, neglecting the damping energy, the maximum values of the strain and kinetic energies are the same. The nodal patterns, including of lateral displacements  $w$ , can be obtained from Eqs. 30.

### Finite-element approach

A finite-element approach allowing the determination of the specific damping capacity of a damped layered composite panel has been proposed by Maheri and Adams [16]. This method can be applied to a honeycomb sandwich panel with composite or aluminium skins.

The strain energy  $U$  is then calculated using the following expression

$$U = \frac{1}{2} \{\delta\}^T [K] \{\delta\} \tag{45}$$

where  $\{\delta\}$  are nodal displacements and  $[K]$  the structural stiffness matrix.

We use here the fact that a mean elasticity matrix  $[D^m]$  can be used to assemble the  $[K]$  matrix with the conventional formulation

$$[K] = \int_V \{[B]^T [D^m] [B]\}_e dV \tag{46}$$

where  $[B]$  is the strain–displacement matrix and the suffix  $e$  refers to the elemental division integrated over the total volume of the structure.

In such a context, if we assume now a parabolic distribution of transverse shear strains through the core thickness, we can write

$$\{\varepsilon_i\} = \left\{ \begin{matrix} \chi_1 z \\ \chi_2 z \\ \chi_4 \left(1 - 4 \frac{z^2}{h^2}\right) \\ \chi_5 \left(1 - 4 \frac{z^2}{h^2}\right) \\ \chi_6 z \end{matrix} \right\} \tag{47}$$



and we can show, using the fact that the following equation

$$\int_V \{\varepsilon_i\}^T [D^m] \{\varepsilon_i\} \{\varepsilon_i\}^T dV = \sum_{k=1}^L \int_{V_k} \{\varepsilon_i\}^T [\bar{Q}_{ij}^k] \{\varepsilon_i\} dV_k \quad (48)$$

must be true, that

$$[D_{ij}^m] = \frac{4}{h^3} \sum_{k=1}^L [\bar{Q}_{ij}^k] (h_k^3 - h_{(k-1)}^3) \quad (i, j = 1, 2, 6) \quad (49a)$$

$$[D_{ij}^m] = \frac{15}{8h} [\bar{Q}_{ij}^c] \left[ h_c - \frac{2h_c^3}{3h^2} + \frac{h_c^5}{h^4} \right] \quad (i, j = 4, 5) \quad (49b)$$

In calculating separately (on a spreadsheet for instance) the symmetric mean elasticity matrix terms, one can define equivalent elastic materials, one for the skin and one for the core, that can be declared and allocated to the corresponding elements in the finite-element model.

Now, in terms of the finite-element formulation, the dissipated energy is given by

$$\Delta U = \frac{1}{2} \{\delta\}^T [K_d] \{\delta\} \quad (50)$$

where  $[K_d]$  is the damped, unsymmetrical structural stiffness matrix given by

$$[K_d] = \int_V \{[B]^T [D_d^m] [B]\}_e dV \quad (51)$$

and  $[D_d^m]$  will be called the damped mean elasticity matrix. The terms of this matrix are defined through the following expression

$$\int_V \{\varepsilon_i\}^T [D_d^m] \{\varepsilon_i\} dV = \sum_{k=1}^L \int_{V_k} \{\varepsilon_i\}^T [\bar{R}_{ij}^k] \{\varepsilon_i\} dV_k \quad (52)$$

By analogy, we have

$$[D_{dij}^m] = \frac{4}{h^3} \sum_{k=1}^L [\bar{R}_{ij}^k] (h_k^3 - h_{(k-1)}^3) \quad (i, j = 1, 2, 6) \quad (53a)$$

$$[D_{dij}^m] = \frac{15}{8h} [\bar{R}_{ij}^c] \left[ h_c - \frac{2h_c^3}{3h^2} + \frac{h_c^5}{h^4} \right] \quad (i, j = 4, 5) \quad (53b)$$

To calculate the dissipated energy  $\Delta U$  using a finite-element software package, the damped structural stiffness matrix  $[K_d]$  must be first assembled. This could be done easily if the  $[\bar{R}]$  matrix was symmetric. The problem can be solved by creating a symmetric damped mean elasticity matrix allowing us to define equivalent materials, one for the skins and one for the core.

The relatively negligible  $[D_{d16}^m]$ ,  $[D_{d26}^m]$ ,  $[D_{d61}^m]$  and  $[D_{d62}^m]$  terms can be ignored and the quite small  $[D_{d12}^m]$  and  $[D_{d21}^m]$  terms can be averaged such that

$$[D_{d12}^m] = [D_{d21}^m] = \frac{[D_{d12}^m] + [D_{d21}^m]}{2} \quad (54)$$

With such modifications, the damped mean elasticity matrix is indeed symmetric.

Using this justified approximation, we now define the equivalent damped elastic properties of the skins as

$$E_x^* = [D_{d11}^m] - \left( \frac{[D_{d12}^m]}{[D_{d22}^m]} \right)^2 [D_{d22}^m], \quad E_y^* = \frac{[D_{d22}^m]}{D_{d11}^m} E_x^*,$$

$$v_{xy}^* = \frac{[D_{d12}^m]}{[D_{d22}^m]} \quad (55)$$

and of the core as

$$G_{xz}^* = [D_{d44}^m], \quad G_{xy}^* = [D_{d55}^m] \quad (56)$$

This method allows, with the same finite-element model and with two different sets of material, data to solve on one hand the eigenvalue problem giving frequency, nodal displacements and strain energy for each mode using the software functionality, and on the other hand a damped structural stiffness matrix  $[K_d]$  taking into account modified equivalent damped materials. A last matrix calculation using the nodal displacements gives  $\Delta U$  and so  $\Psi$  for each mode.

## Experimental

Tests were carried out on two systems of mid-plane symmetric rectangular sandwich plates, namely sandwich plates with CFRP skins, and sandwich plates with aluminium skins, both systems having the same low density, aluminium honeycomb (HC) material as their core. Each composite skin consisted of only 3-ply of CFRP material, with a skin/core thickness ratio of 80 (in the case of the aluminium skins, this ratio was 60). Also, in both systems, the core orthotropic axes were aligned along the plate axes.

The specifications of the sandwich plates tested in the present work are given in Table 1. Definitions of  $a$ ,  $b$  and  $h$  are as those in Fig. 1, and  $t_s$  is the sandwich skin thickness. As shown, the SP1-2 and the SP2-2 plates are, respectively, the same SP1-1 and SP2-1 plates that have been reduced in the side length.

These kinds of composite/aluminium and aluminium/aluminium honeycomb sandwich systems have been used by ALCATEL SPACE as structural panels in telecommunication satellites. The materials that have been used in this experimental phase were supplied by ALCATEL SPACE and are flight representative.

The experimental work essentially consisted of two parts. First, dynamic tests were carried out on the constituent parts of the sandwich panels in order to determine their moduli of elasticity and SDC. These data were then

**Table 1** Specifications of the sandwich plates tested

Plate designation	Composition	<i>a</i> (mm)	<i>b</i> (mm)	<i>h</i> (mm)	<i>t<sub>s</sub></i> (mm)
SP1-1	(+60, 0, -60) CFRP skin, Alum. HC core	500.0	500.0	24.92	0.30
SP1-2	(+60, 0, -60) CFRP skin, Alum. HC core	400.0	400.0	24.92	0.30
SP2-1	Alum. skin, Alum. HC core	501.5	500.5	24.99	0.40
SP2-2	Alum. skin, Alum. HC core	401.0	400.0	24.99	0.40

used to predict the modal characteristics, as described previously. Free-free modal tests were then carried out on sandwich panels as a whole, and the experimental results were compared to the theoretical predictions.

The constituent elastic and damping data were determined in correspondence to the prevalent mode of deformation in the constituent parts when the sandwich is loaded laterally. That is, the skin material was tested for its in-plane properties, whereas the core material was tested for its transverse shear properties.

Sandwich constitutive data

*CFRP composite skins*

The in-plane dynamic properties of the FRP skins were determined by using flexural tests on thin, unidirectional beam samples at 0° and 90° fibre orientation in order to determine the damping and Young’s moduli in these two principal orientations. A torsion test was used on unidirectional beam sample at 0° and 90° orientation in order to determine the longitudinal and transverse shear moduli and damping. The details of these test procedures have been given elsewhere [9]. In order to verify the soundness of the samples and the damping test set-up and procedure, all samples were tested over a range of stress amplitudes and the SDC was observed to be effectively independent of vibration amplitude.

In Table 2, the constitutive elastic and damping data of the composite material are listed.

*Aluminum skins*

Dynamic Young’s modulus was determined from the natural frequency of the aluminium beam samples, which

**Table 2** Dynamic orthotropic elastic and damping properties of the CFRP material used for the sandwich skins

<i>E</i> <sub>1</sub> (GPa)	<i>E</i> <sub>2</sub> (GPa)	<i>G</i> <sub>12</sub> (GPa)	<i>v</i> <sub>12</sub>	<i>ψ</i> <sub>1</sub> (%)	<i>ψ</i> <sub>2</sub> (%)	<i>ψ</i> <sub>12</sub> (%)	<i>ρ</i> (kg/m <sup>3</sup> )
271.0	6.02	5.46	0.34	0.45	7.30	8.16	1563.3

1 is the fibre direction and 2 is transverse to this direction

material was used for the aluminium skin of the all-aluminium sandwich plate. Because the beam samples supplied were thin and soft, it was not possible to conduct resonance flexural and torsion tests on these samples and, consequently, the shear modulus and damping data could not be generated for this material. However, aluminium being an isotropic material whose elastic properties are strain-rate independent, the shear modulus was found from the Young’s modulus and Poisson’s ratio, assuming a value of 0.35 for the latter. Furthermore, aluminium has very low damping, and the damping value previously measured for a high-strength aluminium alloy was also used for the present purposes. In Table 3, the elastic and damping data used for sandwich aluminium skins are listed.

*Aluminum honeycomb core*

Dynamic transverse shear properties of the honeycomb core were determined by conducting shear tests on honeycomb material in the two principal *x* and *y* directions, that is along and across the ‘nodes’ (double-walled webs), respectively. The details of the honeycomb test procedure can be found in [8]. Tests were conducted on several samples in each direction, and the results from those samples that showed non-linear damping (due to cracks and other flaws introduced in manufacturing the test specimens) were discarded.

In Table 4, the constitutive elastic and damping data of the aluminium honeycomb material are listed.

**Table 3** Elastic and damping data used for the aluminium skins of the all-aluminium sandwich

<i>E</i> (GPa)	<i>G</i> (GPa)	<i>ψ</i> <sub>1,2</sub> (%)	<i>ψ</i> <sub>12</sub> (%)	<i>ρ</i> (kg/m <sup>3</sup> )
68.7	25.40	0.10	0.10	2687.1

**Table 4** Dynamic transverse shear elastic and damping properties of the aluminium honeycomb material used for the sandwich core

<i>G</i> <sub>13</sub> (MPa)	<i>G</i> <sub>23</sub> (MPa)	<i>ψ</i> <sub>13</sub> (%)	<i>ψ</i> <sub>23</sub> (%)
140.0	75.4	0.74	1.02

## Sandwich plate modal properties

The sandwich plates were subjected to free-free modal tests. The free-free plate modal tests are primarily used for qualitative purposes and are aimed at establishing the damping properties of the typical plate under various modal deformations.

Unless otherwise stated, the tests were carried out using the test method described by Maheri and Adams [1, 16]. Both bandwidth and free-decay methods were used for the damping measurements, the choice of the method being dependent on the suitability of each method for each particular test. Furthermore, in all the plate tests, the linearity of the variation of SDC with displacement amplitude was verified by using a simple and quick method in which the output voltage from the vibration pickup device was observed to vary linearly with the input current to the vibration drive device.

The experimentally obtained modal characteristics were subsequently compared with theoretically predicted results and NASTRAN finite element model results. The mode shapes shown in the following results are all theoretical mode shapes although, as will be explained later, in most cases these could be verified experimentally.

### Sandwich with CFRP composite skins

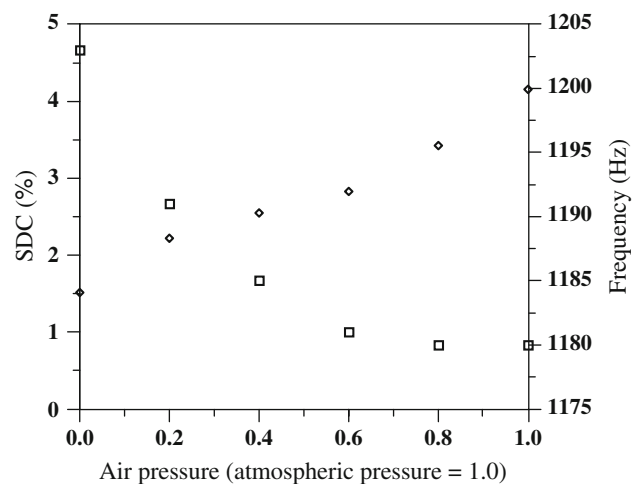
In testing composite skin sandwich panels, substantial damping was observed which was not predicted by theory. As the results in Table 5 show, there is a large discrepancy between the experimental and the predicted damping results, especially in the second mode. The amount of damping in the subsequent modes was so large that it effectively hindered obtaining the resonance frequencies and mode shapes with any degree of certainty. However, as the table shows, the frequency values of those modes that could be established experimentally, namely the first and

the second mode, are reasonably close to the theoretical values.

The large amount of damping was attributed to air-damping (see below). To verify this, a test was conducted in a vacuum chamber whereby the pressure was reduced to 1 millitorr in several steps; at each step the SDC of the second mode of vibration of the plate was measured. Because of the size limitation of the vacuum chamber, the size of the plate was reduced from a 500 (mm) to a 400 (mm) square plate, the latter referred to here as the SP1-2 plate. The test results are plotted in Fig. 2.

As the test results in Fig. 2 show, in this particular case, air-damping has caused an almost threefold increase in the SDC, while the frequency has fallen by about 2%.

Generally, if a stiff, heavy plate vibrates in air, there is little or no effect of the air on the natural frequencies and damping. Even in water, the effect can be very small.



**Fig. 2** Variation of damping and frequency with air pressure for the second mode of the SP1-2 plate with CFRP skins (+60, 0, -60) and aluminium honeycomb core. ◇ SDC; □ frequency

**Table 5** Modal results of the SP1-1 plate, tested in air

Mode shape				
Freq. (Hz)				
Experiment	518	779	–	–
Rayleigh–Ritz Method	531	816	989	1259
SDC (%)				
Experiment	3.79	15.1	–	–
Rayleigh–Ritz Method	1.38	0.83	0.84	0.94

However, when a ‘light’ plate vibrates, the mass and stiffness of the adjacent air can be significant, and acoustic radiation (air-damping) can account for a large proportion of the vibrational energy. The effect is pronounced when the dimensions of the plate (and hence also the nodal patterns) are in approximate coincidence with the wavelength of sound waves in air. At 1000 (Hz), the wavelength of these sound waves is approximately 330 (mm), which is close to the plate dimensions. At reduced pressure, the acoustic radiation is reduced.

Following the above test, all the modal tests on the plate were conducted in vacuum. The in vacuo results are given in Table 6.

Comparing the results in Tables 5 and 6, it is evident that the large discrepancy observed between the experimental and theoretical damping values when testing in air was, indeed, due to air-damping. Furthermore, close correlation is observed between the experimental, theoretical and finite-element model frequencies, and the damping values are also reasonably close in the majority of cases. Due to technical difficulties posed in verifying the in vacuo experimental mode shapes, we could only be certain of those mode shapes that could be established in air. These include the first three modes listed in Table 6.

It is further noted that, by the nature of the test, the in vacuo tests involve attaching a component of the vibration drive mechanism to the plate. In the present case, a small magnet whose mass was less than 2% of the plate was attached. Although this is not expected to change the frequencies and mode shapes significantly, it is nevertheless important to note that it will have some influence on the experimental results, in particular, it is likely to reduce slightly the experimental frequencies, but should have little effect on the damping, excepting in so far as the mode shape was also changed.

*Sandwich with aluminum skins*

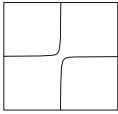
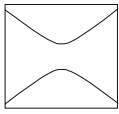
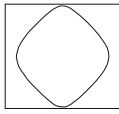

Although substantial air-damping was also experienced with the all-aluminium sandwich plate, unlike the composite sandwich, establishing the in-air modal properties of the aluminium sandwich proved to be much easier. The modal properties could be obtained for all the modes considered, and these are given in Table 7. From the results in this table, it is noted that reasonably good correlation exists between the experimental and Rayleigh–Ritz predicted frequencies although, as mentioned above, air-damping is seen to have again dominated the experimental damping values.

To establish the extent of the influence of air-damping in the damping results of all-aluminium sandwich, the latter was also tested in vacuum. The in vacuo results are given in Table 8.


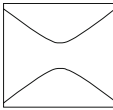
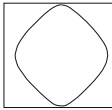
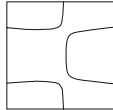
As the table shows, reasonably close correlation exists between the experimental, Rayleigh–Ritz and NASTRAN modal frequencies and damping values.

It may be instructive to consider the inherent sandwich damping, as reflected in the in vacuo results of Tables 6 and 8, in light of a few underlying facts regarding the damping mechanism at work in a sandwich configuration. Generally speaking, the size factor can have a significant influence on the damping in thick plates, particularly in plates that are in sandwich form. The influence of the size factor on damping is proportional to the degree of the difference between the elastic and damping properties of the sandwich constituent parts [17]. This is because the sandwich size, whether thickness-wise or, inversely equivalently, broadness-wise, determines the proportion of the contribution of the skin and of the core to the overall strain and damping energies and, by inference, so does the degree of the difference in the elastic and

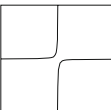
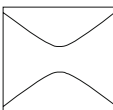
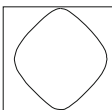
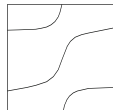
**Table 6** Modal results of the SP1-2 plate, tested in vacuo

Mode shape				
Freq. (Hz)				
Experiment	757	1202	1471	1755
Rayleigh–Ritz method	796	1221	1469	1817
NASTRAN model	750	1140	1381	1655
SDC (%)				
Experiment	1.11	1.51	1.06	1.21
Rayleigh–Ritz method	1.39	0.84	0.84	0.94
NASTRAN model	1.03	1.00	0.76	0.97

**Table 7** Modal results of the SP2-1 plate, tested in air

Mode shape				
Freq. (Hz)				
Experiment	397	613	771	955
Rayleigh–Ritz method	394	608	755	946
SDC (%)				
Experiment	0.90	3.10	22.0	10.5
Rayleigh–Ritz method	0.29	0.18	0.27	0.33

**Table 8** Modal results of the SP2-2 plate, tested in vacuo

Mode shape				
Freq. (Hz)				
Experiment	599	932	1151	1413
Rayleigh–Ritz method	591	913	1122	1367
NASTRAN model	586	895	1107	1326
SDC (%)				
Experiment	0.35	0.37	0.33	0.33
Rayleigh–Ritz method	0.36	0.22	0.33	0.39
NASTRAN model	0.24	0.23	0.25	0.36

damping properties between these two constituent parts. For the same reason, the frequency of vibration and the particular modal deformation that the sandwich undergoes, as well as the plate boundary conditions can all be expected to influence the overall sandwich damping. The fact that the SDC in the all-aluminium sandwich (Table 8) is almost invariant of the modal deformation is the reflection of the fact that not only the skin material is isotropic and its elastic and damping properties are invariant of direction (Table 3), but also that these properties are of the same order of magnitude in the core (Table 4). By contrast, the elastic and damping properties of the CFRP material used in the skin of the composite/honeycomb sandwich are significantly orientation dependent (Table 2). However, it should also be born in mind that by the nature of the present CFRP skin lay-up, which comprises three layers at (+60, 0, -60) orientations, the CFRP skin material is in fact planar-isotropic, and any anisotropy in the skin deformation is limited to the out of plane deformations which have been assumed to be

negligible here. As a result, although the variation in modal damping values of this plate (Table 6) is larger than that in the all-aluminium sandwich, nevertheless, it is relatively little affected by the particular mode of deformation.

## Conclusions

It was shown that it is possible to predict modal characteristics, including damping, of practical sandwich panels using basic laminae theory and a simplified plate deformation analysis. A first-order shear deformation theory was used, although the transverse shearing in a relatively thin sandwich skin was considered to be negligible. Test results tend to suggest that this was a justified assumption, at least in so far as modal characteristics of thin-skinned, free-free sandwich panels are concerned.

The Rayleigh–Ritz expressions used for the present case are a fairly straightforward extension of the classical

method, namely the addition of the two transverse shear rotations to the lateral displacement as the trial functions. Although the derivations and subsequent computer codification are inevitably more voluminous, and notwithstanding the fact that the application of the method is limited to rectangular plates, this numerical method is known to be fast and accurate where it can be applied.

A finite-element approach using NASTRAN software package capabilities has also been used and gives results which are close to the Rayleigh–Ritz and experimental values.

In modal testing of the sandwich panels, it was shown that these experienced enormous damping when tested in air, owing to acoustic radiation. It was concluded, therefore, that in order to obtain data for modal damping due to the inherent damping of the material in sandwich panels, which data that should be of particular interest in space applications, tests will have to be carried out in vacuo.

Both the analytical Rayleigh–Ritz method and the NASTRAN finite-element approach have given quite satisfactory results for both frequencies and specific damping capacities for specific free-free in vacuo tests using two kinds of ALCATEL SPACE sandwich aluminium panels (aluminium skins and CFRP skins).

### Appendix

Components of the Rayleigh–Ritz stiffness matrix

$$\begin{aligned}
 C_{11} &= \sum_{i=1}^M \sum_{j=1}^N \left\{ A_{44} \int_a w_i w_m dx \int_b w'_i w'_n dy \right. \\
 &\quad + A_{55} \int_a w'_i w'_m dx \int_b w_j w_n dy \\
 &\quad + A_{45} \left[ \int_a w'_i w_m dx \int_b w_j w'_n dy \right. \\
 &\quad \left. \left. + \int_a w'_m w_i dx \int_b w_n w'_j dy \right] \right\} \\
 C_{12} &= \sum_{i=1}^M \sum_{j=1}^N \left\{ A_{55} \int_a \psi_m w'_i dx \int_b w_n w_j dy \right. \\
 &\quad \left. + A_{45} \int_a \psi_m w_i dx \int_b w_n w'_j dy \right\} \\
 C_{13} &= \sum_{i=1}^M \sum_{j=1}^N \left\{ A_{44} \int_a w_m w_i dx \int_b \psi_n w'_j dy \right. \\
 &\quad \left. + A_{45} \int_a w_m w'_i dx \int_b \psi_n w_j dy \right\}
 \end{aligned}$$

$$\begin{aligned}
 C_{21} &= \sum_{i=1}^M \sum_{j=1}^N \left\{ A_{55} \int_a \psi_i w'_m dx \int_b w_j w_n dy \right. \\
 &\quad \left. + A_{45} \int_a \psi_i w_m dx \int_b w_j w'_n dy \right\} \\
 C_{22} &= \sum_{i=1}^M \sum_{j=1}^N \left\{ D_{11} \int_a \psi'_i \psi'_m dx \int_b w_j w_n dy \right. \\
 &\quad + D_{16} \left[ \int_a \psi'_i \psi_m dx \int_b w_j w'_n dy \right. \\
 &\quad \left. + \int_a \psi'_m \psi_i dx \int_b w_n w'_j dy \right] \\
 &\quad + D_{66} \int_a \psi_i \psi_m dx \int_b w'_j w'_n dy \\
 &\quad \left. + A_{55} \int_a \psi_i \psi_m dx \int_b w_j w_n dy \right\} \\
 C_{23} &= \sum_{i=1}^M \sum_{j=1}^N \left\{ D_{12} \int_a \psi'_i w_m dx \int_b \psi'_n w_j dy \right. \\
 &\quad + D_{16} \int_a \psi'_i w'_m dx \int_b w_j \psi_n dy \\
 &\quad + D_{26} \int_a w_m \psi_i dx \int_b \psi'_n w'_j dy \\
 &\quad + D_{66} \int_a \psi_i w'_m dx \int_b w'_j \psi_n dy \\
 &\quad \left. + A_{45} \int_a \psi_i w_m dx \int_b w_j \psi_n dy \right\} \\
 C_{31} &= \sum_{i=1}^M \sum_{j=1}^N \left\{ A_{44} \int_a w_i w_m dx \int_b \psi_j w'_n dy \right. \\
 &\quad \left. + A_{45} \int_a w_i w'_m dx \int_b \psi_j w_n dy \right\} \\
 C_{32} &= \sum_{i=1}^M \sum_{j=1}^N \left\{ D_{12} \int_a \psi'_m w_i dx \int_b \psi'_j w_n dy \right. \\
 &\quad + D_{16} \int_a \psi'_m w'_i dx \int_b w_n \psi_j dy \\
 &\quad + D_{26} \int_a w_i \psi_m dx \int_b \psi'_j w'_n dy \\
 &\quad + D_{66} \int_a \psi_m w'_i dx \int_b w'_n \psi_j dy \\
 &\quad \left. + A_{45} \int_a \psi_m w_i dx \int_b w_n \psi_j dy \right\}
 \end{aligned}$$

$$\begin{aligned}
C_{33} = & \sum_{i=1}^M \sum_{j=1}^N \left\{ D_{22} \int_a w_i w_m dx \int_b \psi'_j \psi'_n dy \right. \\
& + D_{26} \left[ \int_a w_i w'_m dx \int_b \psi'_j \psi_n dy \right. \\
& \left. + \int_a w_m w'_i dx \int_b \psi'_n \psi_j dy \right] \\
& + D_{66} \int_a w'_i w'_m dx \int_b \psi_j \psi_n dy \\
& \left. + A_{44} \int_a w_i w_m dx \int_b \psi_j \psi_n dy \right\} \\
& (m = 1, 2, \dots, M; \quad n = 1, 2, \dots, N)
\end{aligned}$$

Components of the Rayleigh–Ritz mass matrix

$$\begin{aligned}
m_{11} &= \sum_{i=1}^M \sum_{j=1}^N \rho h \left[ \int_a w_i w_m dx \int_b w_j w_n dy \right] \\
m_{22} &= \sum_{i=1}^M \sum_{j=1}^N \rho \frac{h^3}{12} \left[ \int_a \psi_i \psi_m dx \int_b w_j w_n dy \right] \\
m_{33} &= \sum_{i=1}^M \sum_{j=1}^N \rho \frac{h^3}{12} \left[ \int_a w_i w_m dx \int_b \psi_j \psi_n dy \right] \\
& (m = 1, 2, \dots, M; \quad n = 1, 2, \dots, N)
\end{aligned}$$

## References

1. Maheri MR, Adams RD (2003) J Sound Vibr 259(1):17. doi: [10.1006/jsvi.2002.5151](https://doi.org/10.1006/jsvi.2002.5151)
2. Yuan WX, Dawe DJ (2002) Intl J Numer Meth Eng 54:195. doi: [10.1002/nme.411](https://doi.org/10.1002/nme.411)
3. Chen Q, Chan YW (2000) Comput Struct 74:51. doi: [10.1016/S0045-7949\(98\)00321-6](https://doi.org/10.1016/S0045-7949(98)00321-6)
4. Noor AK, Burton WS, Bert CW (1996) Appl Mech Rev Trans ASME 49(3):155
5. Nayak AK, Sheno RA, Moy SSJ (2002) IMechE, J Mech Eng Sci 216:591
6. Nayak AK, Moy SSJ, Sheno RA (2003) J Strain Anal Eng Design 38:377. doi: [10.1243/03093240360713441](https://doi.org/10.1243/03093240360713441)
7. Rikards R, Chate A, Korjakin A (1995) Eng Comput 12:61
8. Adams RD, Maheri MR (1993) Compos Sci Technol 47(1):15. doi: [10.1016/0266-3538\(93\)90091-T](https://doi.org/10.1016/0266-3538(93)90091-T)
9. Adams RD, Maheri MR (1994) Compos Sci Technol 50(4):497. doi: [10.1016/0266-3538\(94\)90058-2](https://doi.org/10.1016/0266-3538(94)90058-2)
10. Dawe DJ, Roufaeil OL (1980) J Sound Vibr 69(3):345. doi: [10.1016/0022-460X\(80\)90477-0](https://doi.org/10.1016/0022-460X(80)90477-0)
11. Craige TJ, Dawe DJ (1986) Intl J Solid Struct 22(2):155. doi: [10.1016/0020-7683\(86\)90005-3](https://doi.org/10.1016/0020-7683(86)90005-3)
12. Adams RD, Bacon DGC (1973) J Compos Mater 7:402
13. Young D (1950) J Appl Mech 17:448
14. Ashton JE, Waddoups ME (1969) J Compos Mater 3:148. doi: [10.1177/002199836900300111](https://doi.org/10.1177/002199836900300111)
15. Ashton JE, Whitney JM (1970) Theory of laminated plates. Technomic Publishing Company, Conn, USA
16. Maheri MR, Adams RD (1995) Compos Sci Technol 55(1):13. doi: [10.1016/0266-3538\(95\)00074-7](https://doi.org/10.1016/0266-3538(95)00074-7)
17. Maheri MR (1991) Vibration damping in composite/honeycomb sandwich beams, PhD thesis, Department of Mechanical Engineering, University of Bristol